J Ginseng Res 45 (2021) 86–97

Contents lists available at ScienceDirect

Journal of Ginseng Research

journal homepage: http://www.ginsengres.org

Research Article

Purification of ginseng rare sapogenins 25-OH-PPT and its hypoglycemic, antiinflammatory and lipid-lowering mechanisms

Jing Xu [1,☆], Hairong Liu [1,☆], Guangyue Su [1,4], Meng Ding [1], Wei Wang [1], Jincai Lu [2,***], Xiuli Bi [3,**], Yuqing Zhao [1,4,*]

[1] School of Functional Food and Wine, Shenyang Pharmaceutical University, Shenyang, Liaoning, China
[2] Department of Medicinal Plant Shenyang Pharmaceutical University, Shenyang, Liaoning, China
[3] School of Life Science, Liaoning University, Shenyang, Liaoning, China
[4] Key Laboratory of Structure-based Drug Design and Discovery of Ministry of Education, Shenyang Pharmaceutical University, Shenyang, Liaoning, China

ARTICLE INFO

Article history:
Received 13 September 2018
Received in Revised form
21 October 2019
Accepted 1 November 2019
Available online 9 November 2019

Keywords:
Ginseng
Insulin resistance
Macroporous resin
T2DM

ABSTRACT

Background: Panax ginseng Meyer has been used as a nourishing edible herb in East Asia for thousands of years. 25-OH-PPT was first discovered as a natural rare triterpenoid saponin in ginseng stems and leaves by our group. Research found that it showed strong inhibitory effects on α-glucosidase and protein tyrosine phosphatase 1B, and protected cardiocytes (H9c2) through PI3K/Akt pathway.
Methods: In the research, in order to optimize the 25-OH-PPT enrichment process, optimal macroporous resins and optimal purification conditions were studied. Meanwhile, the hypoglycemic effect and mechanism of 25-OH-PPT were evaluated by using STZ to establish insulin-dependent diabetic mice and the spontaneous type 2 diabetes DB/DB mice.
Results and Conclusion: Research found that 25-OH-PPT can reduce blood glucose and enhance glucose tolerance in STZ model mice. It increases insulin sensitivity by upregulating GLUT4 and AMPK in skeletal muscle, and activating insulin signaling pathways. In DB/DB mice, 25-OH-PPT achieves hypoglycemic effects mainly by activating the insulin signaling pathway. Meanwhile, through the influence of liver inflammatory factors and lipids in serum, it can be seen that 25-OH-PPT has obvious anti-inflammatory and lipid-lowering effects. These results provide new insights into the study of ginseng as a functional food.

1. Introduction

Diabetes mellitus (DM) is an important metabolic disease that is increasing in prevalence and threatening human health [1]. It is the third most common cause of death after heart disease and cancer. The main pathophysiological features of diabetes are insulin resistance and defects in insulin secretion in liver, skeletal muscle and adipose tissue [2]. These abnormalities produce an imbalance in glucose metabolism and elevated blood glucose concentrations. At present, treatment of diabetes centers upon use of various hypoglycemic drugs and direct insulin receptor substrate [3]. However, long-term use of these drugs increases the burden on some organs, such that organ damage caused by antidiabetic drug toxicity cannot be ignored [4]. There has been increasing research and development into antidiabetic drugs including medicinal plants that have a favorable effect profile and the ability to treat

Abbreviations: DM, diabetes mellitus; AMPK, adenylate-activated protein kinase; T2DM, type 2 diabetes mellitus; IRS-1, insulin receptor substrate-1; IR, insulin receptor; GLUT4, glucose transporter 4; 25-hydroxyl-protopanaxatriol, 25-OH-PPT, 20 (R)-dammaran-3β, 6α, 12β, 20, 25-pentol; STZ, streptozotocin; IPGTT, intraperitoneal glucose tolerance test; AUC, area under the curve; TG, triglycerides; TC, total cholesterol; IL-1, interleukin-1; IL-6, interleukin-6; COX2, cyclo-oxygenase 2; TNF-α, tumor necrosis factor-α; BCA, bicinchoninic acid; INSR, insulin receptor; BSA, bovine serum albumin.

* Corresponding author. School of Functional Food and Wine, Shenyang Pharmaceutical University, No.103, Wenhua Road, Shenhe District, Shenyang 110016, Liaoning, PR China.
** Corresponding author. School of Life Science, Liaoning University, Chongshan Middle Road No.66, Huanggu District, Shenyang 110036, Liaoning, PR China.
*** Corresponding author. Department of Medicinal Plant, Shenyang Pharmaceutical University, No.103, Wenhua Road, Shenhe District, Shenyang 110016, Liaoning, PR China.
E-mail addresses: jincailu@126.com (J. Lu), xiulibi@gmail.com (X. Bi), zyq4885@126.com (Y. Zhao).
☆ This authors contributed equally to this work.

https://doi.org/10.1016/j.jgr.2019.11.002
p1226-8453 e2093-4947/$ – see front matter

complications [5]. Development of diabetes is related closely to multiple factors in the glucose metabolic pathway. Adenylate-activated protein kinase (AMPK) is a protein kinase that is important for regulating cell energy [6]. It is a key target for the treatment of diabetes, as it plays a regulatory role in many aspects that are relevant to type 2 diabetes mellitus (T2DM) including insulin secretion, islet cell damage, glycogen synthesis and gluconeogenesis. Insulin receptor substrate-1 (IRS-1), IRS and insulin receptor (IR) are key proteins in the insulin signaling pathway, which synergistically regulate blood glucose in the body. At molecular levels, complex relationship exists between the AMPK and insulin signaling pathways. For instances, AMPK has been reported to regulate IRS-1 [7] and Akt/PKB [8], while insulin and Akt have negative impacts on AMPK activation [9]. Therefore, we have investigated the AMPK and insulin signaling together. Glucose transporter 4 (GLUT4), a member of the glucose transporter family, is responsible for glucose transport to the cell membrane for metabolism in muscle and adipose tissue. The transport of GLUT4 is dominated by two major signaling pathways, the insulin signaling pathway and the AMPK signaling pathway. It is very necessary to study GLUT4 through which way function can be activated.

Panax ginseng Meyer is a perennial herb native to Korea and China [10]. Ginseng is one of the most important plants in the *Ginseng* genus. Its content is very complex, and it is rich in ginsenosides, ginseng polysaccharides, ginseng proteins, amino acids, flavonoids and other substances. Modern pharmacological studies have shown that the main active ingredient is ginsenoside, which has various pharmacological effects including regulating immunity, anticancer and antiaging. It is also used in the treatment of cardiovascular diseases, dementia and liver protection. In modern research, ginsenosides, ginseng polysaccharides and other ginseng constituents have been shown to significantly lower blood glucose concentrations [11]. For ginsenosides, this effect is mediated via multiple pathways and targets, and with important advantages compared with chemical drugs [12]. However, due to the complex composition of ginseng and the potential for constituents to be synergistic or antagonistic with each other, it is important to ascertain the effective components that exert sustained and effective hypoglycemic effects.

In 1990, our group isolated a new triterpenoid from ginseng stems and leaves for the first time [13] and determined its structure as 20 (R)-dammaran-3β, 6α, 12β, 20, 25-pentol, (25-hydroxyl-protopanaxatriol, 25-OH-PPT) (Fig. 1). In 2008, column chromatography was used to separate 25-OH-PPT from the ginseng fruit saponin hydrolysates [14], panax notoginseng stem saponin hydrolysates [15] and saponin hydrolysates from the basal part of the panax notoginseng stem [16]. The hypoglycemic activity test of 25-OH-PPT *in vitro* showed that it exhibited stronger inhibition of α-glucosidase and protein tyrosine phosphatase-1B activities than their positive control acarbose and Na_3VO_4 [17]. Hu et al. compared the content of 25-OH-PPT in different sources by reversed-phase high performance liquid chromatography system (ELSD-HPLC). The amount present in each different part was small, except the ginseng stems and leaves which had a large enough 25-OH-PPT content. Because of the cheapness of ginseng stems and leaves, it can be used for in-depth research and development [18].

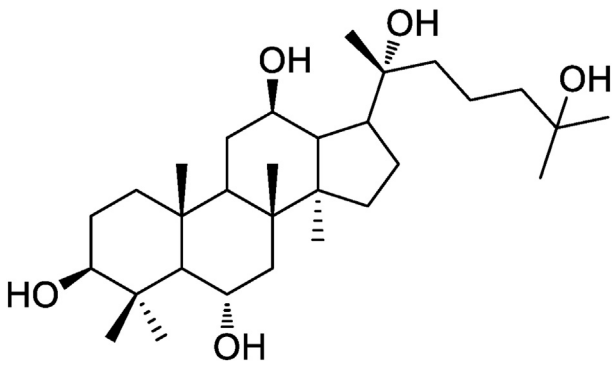

Fig. 1. The chemical structure of 25-OH-PPT.

Macroporous resin has been widely used in the industrial production of natural products because of its good selectivity, large adsorption capacity, fast adsorption speed, high production efficiency, easy desorption, low solvent consumption, low cost, easy operation and renewability [19,20]. Therefore, the number and variety of various commercial macroporous resins are increasing to improve the current status of industrial separation. Although the use of macroporous resins for the separation and purification of ginsenosides has been reported, it is rarely seen that the separation and purification of the monomers can be obtained with high purity.

In this study, a green, safe and nontoxic process preparation method was established, which is suitable for industrial production, and has a low cost. The preferred separation process can obtain a monomer compound with high purity. It achieves a new breakthrough in separation and purification with macroporous resin. We also research the effects of 25-OH-PPT on streptozotocin (STZ)-induced diabetes mice and DB/DB mice's body weight, blood glucose and so on. At the same time, the hypoglycemic mechanism of 25-OH-PPT was researched, and it was found that it has the ability to alleviate diabetic complications.

2. Materials and methods

2.1. Samples

Ginseng stem and leaf saponin was obtained from Liaoning Fushun Xintai Ginseng Health Care Product Co., Ltd. (Fushun, China).

2.2. Chemicals and reagents

25-OH-PPT (purity >98.0%) was made by our group. Methanol (chromatographic grade) was purchased from Concord Chemical Reagents Co. (Tianjin, China). Ethanol was analytical grade and was obtained from Yongda Chemical Reagent Co., Ltd. (Tianjin, China). The water used for HPLC analysis and sample preparation was from Wahaha Group Co., Ltd. (Hangzhou, China).

For the standard solution, an appropriate amount of 25-OH-PPT was dissolved in methanol to obtain a concentration of 0.5 mg/mL. All solutions ready for HPLC analysis were filtered through a 0.45 μm microfilter before injection.

2.3. Preparation of ginseng stem and leaf saponin acid hydrolysate

Ginseng stem and leaf saponin (10 g) was extracted with 100 mL of 40% hydrochloric acid (v/v) using ultrasound for 0.5 h in a sonication water bath (KQ2200B, Kunshan Ultrasonic Equipment Co., Ltd., Kunshan, China), the sodium hydroxide was precipitated and the extracts were combined and centrifuged at 3000 rpm for 10 min. Centrifugation and water washing were used to remove impurities.

2.4. ELSD-HPLC analysis of 25-OH-PPT in acid hydrolysate

A L2000 series reversed-phase high performance liquid chromatography system (Hitachi, Japan) was employed to determine the 25-OH-PPT content. Chromatographic separation was

performed using a Kromasil C18 reverse phase column (250 mm × 4.6 mm, 5 μm). The mobile phase is methanol (eluent A) and water (eluent B). Elution with a mixture of 70% A and 30% B at a flow rate of 1.0 mL/min in 20 min; column oven temperature 35.0°C; evaporation chamber temperature of 87.0°C, carrier gas flow rate of 2.20 L/min; injection volume is 10.0 μL. The quantification was conducted using the 25-OH-PPT standard solution. The calibration curve (five data points) is linear with $R^2 = 0.9992$. All samples used for analysis were filtered through a 0.45 μm membrane prior to injection.

2.5. Experimental animals

C57BL/6 mice were obtained from Liaoning Changsheng Biotechnology Co., Ltd. (China) at four weeks of age. C57BL/KsJ-DB/DB mice and C57BL/KsJ mice were obtained from Nan Jing Better Biotechnology Co., Ltd. (China) at nine weeks of age. The mice were kept in an environmentally controlled breeding room (temperature: 20 ± 2°C, humidity: 60% ± 5%, 12 h light/dark cycle). All mice had free access to tap water. The experiments were carried out with the approval of the Committee of Experimental Animal Administration of Liaoning University.

2.6. Experimental design

Preparation of STZ mice: four-week-old C57/BL male mice were used. One week after adaptive feeding, 1% STZ sodium citrate solution was intraperitoneally injected at a dose of 80 mg/kg body weight for three times, two days apart, to induce a hyperglycemic mice model. After five days, the mice were given venous blood at the end to measure their blood glucose level. The mice with blood glucose values more than 11.6 mmol/L were selected, and mice with polydipsia, polyphagia and polyuria were used as ideal experimental diabetes model.

STZ mice group: at four weeks of age, the mice were divided into five groups (n = 10 each) and treated with normal feeding (normal control), high fat and sugar feeding (STZ mice, model control), 25-OH-PPT (20 mg/kg, STZ mice), 25-OH-PPT (40 mg/kg, STZ mice) and metformin (50 mg/kg, STZ mice) by oral gavage once every two days for four weeks.

DB/DB mice group (evenly grouped according to blood glucose): at nine weeks of age, the mice were divided into four groups (n = 6 each) and treated with normal feeding (C57BL/KsJ mice, normal control), normal feeding (C57BL/KsJ-DB/DB mice, model control), 25-OH-PPT (40 mg/kg, C57BL/KsJ-DB/DB mice) and rosiglitazone (4 mg/kg, C57BL/KsJ-DB/DB mice) by oral gavage once every two days for five weeks.

2.7. Static adsorption/desorption and dynamic adsorption/desorption experiments

In order to study the effect of different resin types on 25-OH-PPT adsorption, four different macroporous resins, AB-8, D101, HPD-100 and HPD-600, were used for static and dynamic adsorption experiments. The following equations are used to quantify adsorption and desorption capacities and desorption rates:

$$q_e = \frac{(C_0 - C_e)}{W} V_i$$

$$D = \frac{C_d V_d}{(C_0 - C_e) V_i} \times 100\%$$

q_e is the adsorption capacity (mg/g resin) when the adsorption equilibrium, C_0 and C_e, are the initial concentration and equilibrium concentration (mg/mL) of 25-OH-PPT in the solution, V_i is the volume of the sample solution (mL), W is the weight of dry resin (g), C_d and V_d are the concentration and volume of 25-OH-PPT after desorption, D is the desorption ratio (%) and C_e and V_i are the same as above.

2.8. Single factor investigation of optimal separation conditions

The effect of sample concentration, adsorption flow rate and macroporous resin column diameter ratio on adsorption efficiency was investigated by single factor experiment. The sample concentrations investigated in the experiment were empirically selected as 10 mg/mL, 20 mg/mL, 30 mg/mL; the adsorption flow rates were 1 BV/h, 2 BV/h, 3 BV/h; and the resin column diameter ratios were 1:20, 1:10, 1:2. When the effluent concentration is detected to be greater than 10% of the original solution, the sample is stopped, the sample volume is recorded and the adsorption amount is calculated.

2.9. Determination of dynamic elution gradient and volume

The prepared hydrolyzed solution was loaded on a macroporous resin column (1.5 × 30 cm, 20 g) to purify 25-OH-PPT. To optimize desorption conditions for 25-OH-PPT, elution was performed using different ethanol concentrations of 10%, 20%, 30%, 40%, 50%, 60%, 70%, 80%, 90% and 100% (v/v). The desorbed 25-OH-PPT concentration in each eluate was analyzed by ELSD-HPLC.

2.10. Measurement of blood glucose and body weight

After one week of dosing, the body weight and fasting blood glucose of the mice were measured. Blood sampling from the tail vein was collected before the meal of the day (after 16 h fasting) to determine the fasting blood glucose (FBG) by the blood glucose meter. The body weights of the mice after weekly dosing and FBG until the end of the dosing period, comparing the significant differences between each group, were recorded [21].

2.11. Intraperitoneal glucose tolerance test (IPGTT)

For the intraperitoneal glucose tolerance test (IPGTT), mice were subjected to fasting overnight for 16 h; their fasting blood glucose was measured and glucose was administered by IP injection. Blood was collected from the tail vein for glucose measurements at 5, 15, 30, 60 and 120 min after glucose injection. The IPGTT curve and the area under the curve (AUC) were analyzed afterward.

2.12. Detection of the effect of 25-OH-PPT on blood lipid changes in diabetic mice by kit method

At the end of the dosing period, 1 mL of blood was collected from the venous plexus of each group of mice, the cells were allowed to stand at room temperature for 30 min and then separated at 4°C, 4000 rpm/min for 15 min. The separated plasma was taken out, placed in a 1.5 mL cryo tube and sealed in a sealed -80°C refrigerator for use.

The triglyceride and total cholesterol levels in the serum of the mice were tested according to the instructions on the triglycerides (TG) and serum total cholesterol (TC) kits (Biosino sincerely Co., Ltd., China), and each sample was tested three times to eliminate systematic errors. The data was analyzed to compare significant differences between groups.

2.13. Effect test of organ index in diabetic mice

At the end of the dosing period, the mice were weighed, and the eyeballs were sacrificed after taking blood. The spleen, liver, kidney and other organs were dissected and weighed. The organ ratio was calculated; the organ index calculation formula: organ index = organ weight/weight × 100%.

2.14. Total RNA extraction, cDNA synthesis and RT-PCR reaction system in mice skeletal muscle

Total RNA was isolated from the skeletal muscle of mice thigh by using Trizol reagent (Sangon Biotech Shanghai Co., Ltd.). The extracted RNA was eluted in 100μL of nuclease-free water and stored at -80°C until use. First-strand cDNA was synthesized using qPCR Reverse Transcriptase Kit (CW Biotech Co., Ltd., Beijing, China) according to the manufacturer's instruction. The reaction mixture contained 1 μL of RNA template, 4 μL of dNTP mix (2.5mM of each), 3μL of primer mix, 4μL of 5 × RT Buffer, 1 μL of SuperRT, 8 μL of RNase-free water (Sangon Biotech Shanghai Co., Ltd.). The reaction was conducted at 42°C for 30—50 min, 85°C for 5min and terminated at 4°C.

PCR was performed in a total of 50 μL reaction using SYBR Green PCR Master Mix (CW Biotech Co., Ltd, Beijing, China) as follows: 25 μL of the UltraSYBR Mixture, 10 μL of the reverse primer, 10 μL of the forward primer, 1 μL of the DNA template and 22 μL of RNase-free water. The reaction was conducted with a 10 min denaturation at 95°C, followed by 40 cycles of 95°C for 10 s, 60°C for 30 s and 72°C for 30 s, terminating at 72°C for 7 min.

Primers used were: Glucose transporter 4 (GLUT4; forward, 5′-CTTGGCTCCCTTCAGTTTGG-3'; reverse, 5′-CTACCCAGCCACGTTG-CATT-3′), Adenylate-activated protein kinase a1 (AMPKa1; forward, 5′-AAGCCGACCCAATGACATCA-3'; reverse, 5′-CTTCCTTCGTA-CACGCAAAT-3′), Beta-actin (Actb; forward, 5′-AGGCAAACCGT-GAAAAGATG-3'; reverse, 5′-AGGCAAACCGTGAAAAGATG-3′).

The methods of the pathological examination, total RNA extraction, cDNA synthesis and RT-PCR reaction system of liver are the same as total RNA extraction, cDNA synthesis and RT-PCR reaction system in mice thigh muscle.

Primers used were: Interleukin-1 (IL-1; forward, 5′GCAACTGTTCCTGAACTCAACT-3'; reverse, 5′ATCTTTTGGGGTCCGT CAACT-3′), Interleukin-6 (IL-6; forward, 5′TAGTCCTTCCTACCCCAA TTTCC-3'; reverse, 5′TTGGTCCTTAGCCACTCCTTC-3′), Cyclo-oxygenase 2 (COX2; forward, 5′-TGAGCAACTATTCCAAACCAGC-3'; reverse, 5′-GCACGTAGTCTTCGATCACTATC-3′), Tumor necrosis factor-α (TNF-α; forward, 5′-CCCTCACACTCAGATCATCTTCT-3'; reverse, 5′-GCTACGACGTGGGCTACAG-3′), Beta-actin (Actb; forward, 5′-AGGCAAACCGTGAAAAGATG-3'; reverse, 5′-AGGCAAACCGTGAAAA-GATG-3′).

2.15. Western blot analysis

The ground mouse thigh muscle tissue was taken, 200 μL of protein lysate was added to lyse on ice for 3 h and then centrifuged at 4°C × 12,000 rpm/min for 15 min at a low temperature high speed centrifuge, and the supernatant was placed in a new EP tube. Five μL of protein sample was taken and its concentration was measured by bicinchoninic acid (BCA) protein concentration kit (Sangon Biotech Shanghai Co., Ltd.) The other protein samples are mixed with 40 μL 5 × Loading Buffer and then denatured in a metal bath at 95°C for 5 min for Western Blot experiment [22].

The denatured protein sample was taken and warmed at 40°C for 10 min before loading. The sample is applied for electrophoresis. The membrane after completion of the transformation was placed in a preformulated 5% BSA solution shaker at room temperature for 3 h and then subjected to antibody incubation. Insulin receptor (INSR), p-INSR, p-IRS-1 (Cell Signaling Technology, Inc., USA) antibodies were diluted 1:1000 with 5% bovine serum albumin (BSA) solution; β-actin (Nanjing, China) antibody was diluted 1:5000; membrane was incubated for 3 h; and membrane was washed with TBST for 30 min × 3 times, secondary antibody 1:3000 incubation after 2.5 h exposure.

2.16. Statistical analysis

The data are expressed as mean ± SEM of three independent experiments. The significant was evaluated using one-way analysis of variance. For all tests, probability values of <0.05 were considered significant.

3. Results and discussion

3.1. Static adsorption investigation results of different resins

Four macroporous resins, HPD-100, HPD-600, AB-8 and D101, were used to enrich 25-OH-PPT from ginsenosides and combine the physical properties of four resins [23]. As depicted in Table 1, AB-8 is weakly polar, HPD-100 and D101 are nonpolar and HPD-600 is polar. According to the principle of “similar absorption,” nonpolar macroporous resins such as HPD-100 and D101 have better adsorption than other types of resins. The pore size and specific surface area of macroporous resins have a great influence on the adsorption effect. The average pore diameter of HPD-100 is smaller than that of D101, and its specific surface area is larger than that of HPD-100. Its adsorption effect is better than that of D101. This shows that the adsorption of macroporous resin to 25-OH-PPT mainly utilizes van der Waals forces or hydrogen bonds between the resin and the substance, and partly utilizes the porous mesh structure and the high specific surface area formed by the molecular sieve.

Through static adsorption and dynamic adsorption (Fig. S1-A, B, supplementary materials), the 25-OH-PPT adsorption and desorption rates were investigated. Four different types of resins were screened. The results showed that the macroporous resin HPD-100 had better adsorption and desorption of 25-OH-PPT. Combined with dynamic adsorption and static adsorption results, the following experiments were conducted using HPD-100 macroporous resin for the purification of 25-OH-PPT in the ginsenoside saponin acid hydrolysates.

3.2. Single factor experiment to determine the best separation conditions

From the results (Fig. S1-C—E, supplementary materials), it can be seen that the sample concentration is large to cause the leakage of the resin column to increase. Considering that the 25-OH-PPT adsorption amount is 20 mg/mL, the mass concentration of the sample solution is preferably 20 mg/mL. It was found that when the

Table 1
Parameters of four different resins

Macroporous resin	AB-8	D101	HPD-100	HPD-600
Polarity	Weak-polar	Nonpolar	Nonpolar	polar
Surface area (m^2/g)	480—520	≥400	650—700	550—600
Average pore diameter (nm)	130—140	100—110	85—90	80
Particle diameter (mm)	0.3—1.25	0.3—1.25	0.3—1.2	0.3—1.2

Table 2
Results of gradient elution of 25-OH-PPT on the HPD-100 resin

Concentration of ethanol (%)	Mass of dried residue (mg)	Mass of 25-OH-PPT (mg)	Content of 25-OH-PPT (%)
0	0.92	-	-
10	2.93	-	-
20	182.54	1.84	1.01
30	94.42	15.84	16.78
40	50.73	40.79	80.41
50	36.72	16.75	45.62
60	88.16	8.37	9.49
70	46.39	2.32	5.00
80	56.94	0.28	0.49
90	35.43	-	-
Acid hydrolysates			12.5

adsorption flow rate was 1 BV/h, the adsorption amount reached the maximum, and thus the final adsorption flow rate was 1 BV/h. When the diameter height ratio of resin column is 1:20, the amount of 25-OH-PPT adsorption reaches the maximum, and therefore it is appropriate to finally determine that the diameter height ratio is 1:20.

The best process for finalizing the enrichment of 25-OH-PPT on HPD-100 resin is adsorption. The best adsorption method is as follows, the concentration of the sample solution was 20 mg/mL, in which the 25-OH-PPT concentration was 2.0833 mg/mL, the adsorption flow rate was 0.5 mL/min and the diameter height ratio of resin column was 1:20.

3.3. Dynamic adsorption/desorption experiments

The dynamic leakage curve of 25-OH-PPT on HPD-100 resin was obtained from the elution volume and the solution concentration. As shown in Fig. S2A (supplementary materials), 25-OH-PPT in the sample solution was almost all adsorbed before 100 mL, and when the leakage process gradually started, as the elution volume increased from 60 to 75 mL, it accelerated sharply. In general, adsorption saturation is defined when the concentration in the effluent is 10% of the original concentration. Therefore, the feed volume of the sample solution that was screened for 25-OH-PPT concentration on the HPD-100 resin was determined to be 60 mL (4 BV).

Dynamic desorption was performed using gradient elution at 1 mL/min. Gradient elution results show different desorption capacities as shown by changes in ethanol concentration during elution. The increase in ethanol concentration leads to an increase in the desorption capacity of 25-OH-PPT, which reaches a maximum at 40% ethanol. If ethanol concentration increases continuously, the concentration of 25-OH-PPT in the eluent drops sharply.

As shown in Fig. S2B (supplementary materials), a large amount of highly purified 25-OH-PPT was found in 40% ethanol-water solution. During the separation and enrichment of HPD-100 macroporous resin, the 25-OH-PPT content can reach 80.41% (Table 2, Fig. 2). The HPLC liquid analysis of ginsenoside hydrolysate and 40% ethanol showed that most of the polar impurities were removed during this elution process. After treatment with HPD-100 macroporous resin, the relative peak area of 25-OH-PPT significantly increased. Therefore 20% ethanol can be used to remove impurities and 40% ethanol is chosen as the 25-OH-PPT enrichment gradient for elution.

3.4. Effect of 25-OH-PPT on fasting blood glucose and body weight

The results are shown in Fig. 3A. In the STZ model, high dose 25-OH-PPT significantly decreased mouse body weight at the fourth week of administration. Compared with the model group, 25-OH-PPT significantly reduced fasting blood glucose concentrations in mice. In DB/DB mice (Fig. 3B), the effect of 25-OH-PPT on body weight was not significant, probably due to the large food intake. Compared with the model group, 25-OH-PPT significantly reduced fasting blood glucose in mice. This effect was most pronounced in the DB/DB mice model, and the hypoglycemic effect was comparable to that of the positive drug.

3.5. Effect of 25-OH-PPT administration on IPGTT in mice

As shown in Fig. 4A, AUC is the area under the two curves, which can reflect the tolerance of mice to glucose. In the IPGTT of STZ-induced hyperglycemic mice, the blood glucose was inhibited after 25-OH-PPT administration, but the effect was not obvious. The dose of STZ used in this experiment caused the destruction of most of the islets in mice, leading to insulin-dependent diabetes mellitus; so it is speculated that the noninsulin drug 25-OH-PPT failed to produce a significant effect. However, in the IPGTT of DB/DB mice (Fig. 4B), it can be seen that the 25-OH-PPT administration can significantly inhibit the rise of blood glucose and enhance the tolerance to glucose. The effect is remarkable at 30 min and 60 min, AUC is more intuitive to observe that 25-OH-PPT significantly enhances the tolerance of mice to glucose.

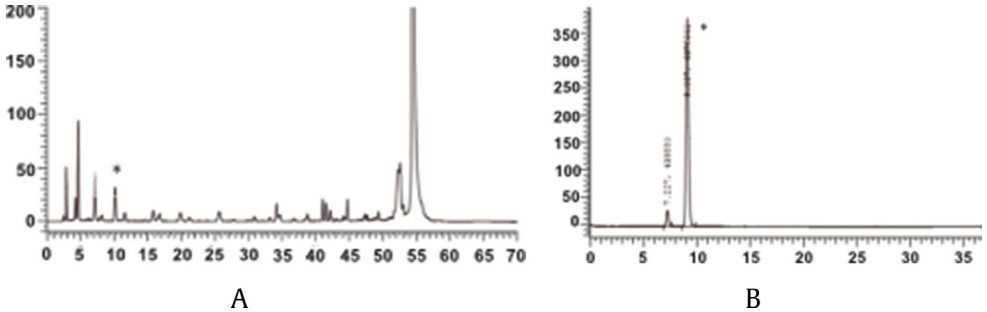

Fig. 2. HPLC chromatograms of the extracts before purification using macroporous resins (**A**); 25-OH-PPT (T19) after recrystallization from methanol (**B**). The peak indicated with an asterisk (*) is the 25-OH-PPT peak.

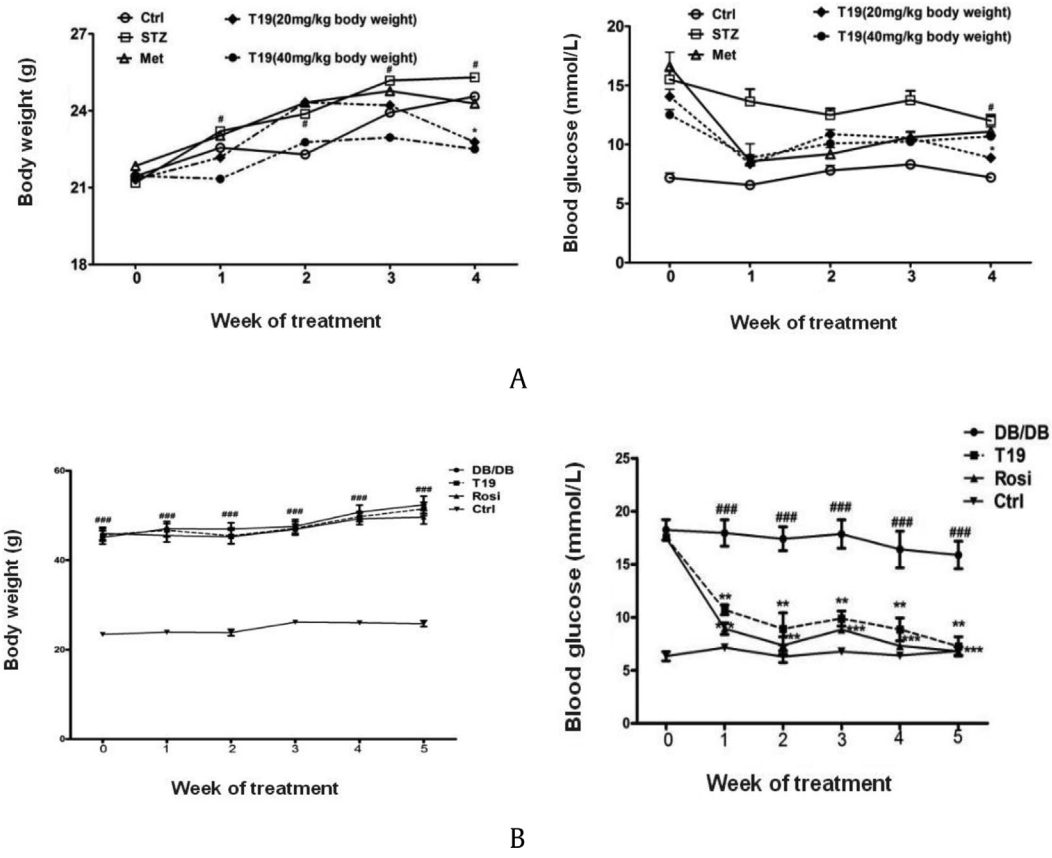

Fig. 3. Effect of 25-OH-PPT (T19) on body weight; blood glucose in STZ-induced hyperglycemic mice (n = 10/group) (**A**) and DB/DB mice (n = 6/group) (**B**) (Values are expressed as mean ± SEM of three independent experiments. $^{*}p < 0.05$ vs. ctrl, $^{**}p < 0.01$ vs. ctrl, $^{\#}p < 0.05$ vs. model, $^{\#\#}p < 0.01$ vs. model.)

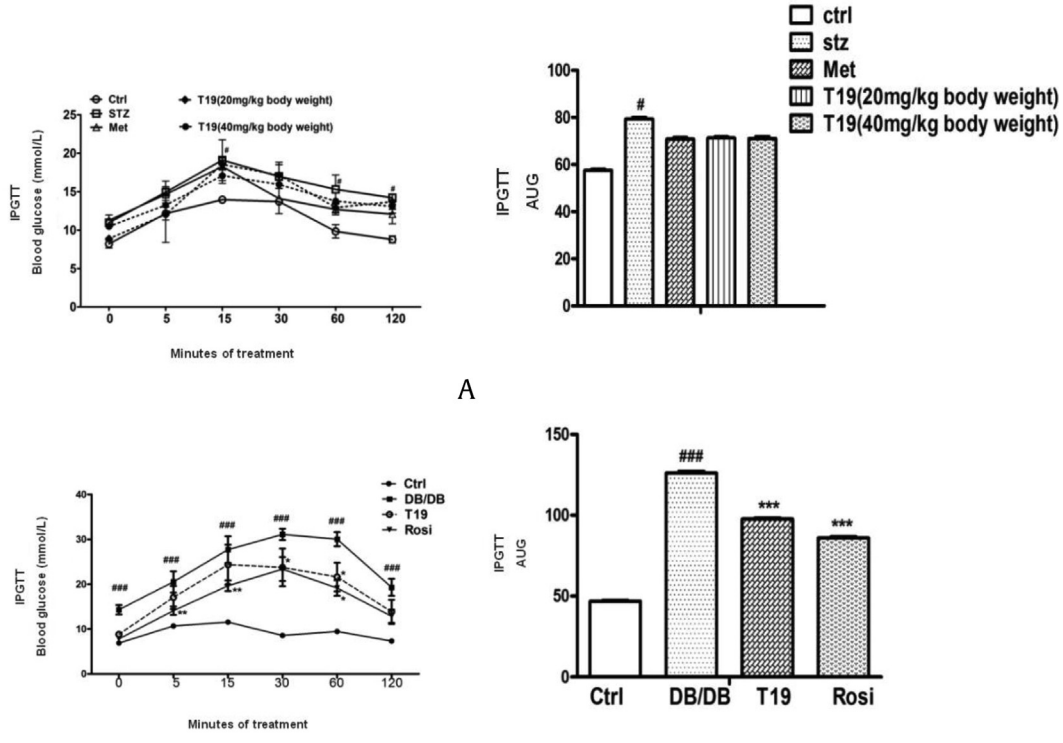

Fig. 4. Effect of 25-OH-PPT (T19) on IPGTT in STZ-induced hyperglycemic mice (n = 10/group) (**A**) and DB/DB mice (n = 6/group) (**B**) (Values are expressed as mean ± SEM of three independent experiments. $^{*}p < 0.05$ vs. ctrl, $^{**}p < 0.01$ vs. ctrl, $^{\#}p < 0.05$ vs. model, $^{\#\#}p < 0.01$ vs. model.)

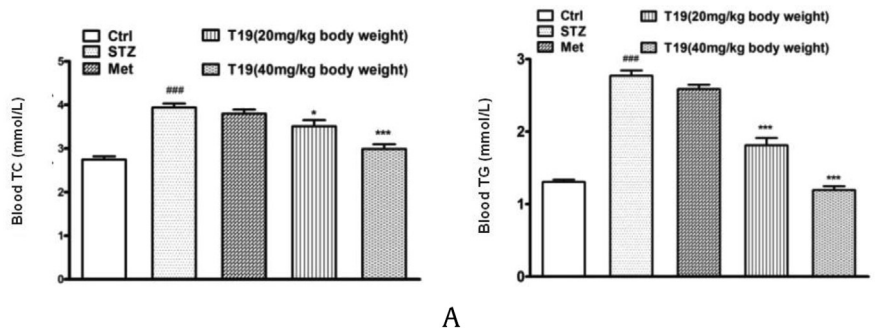

A

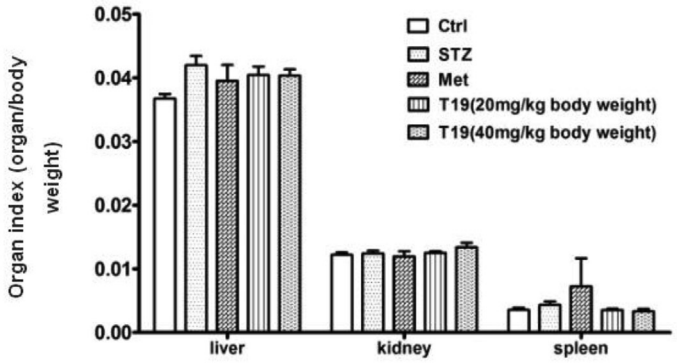

B

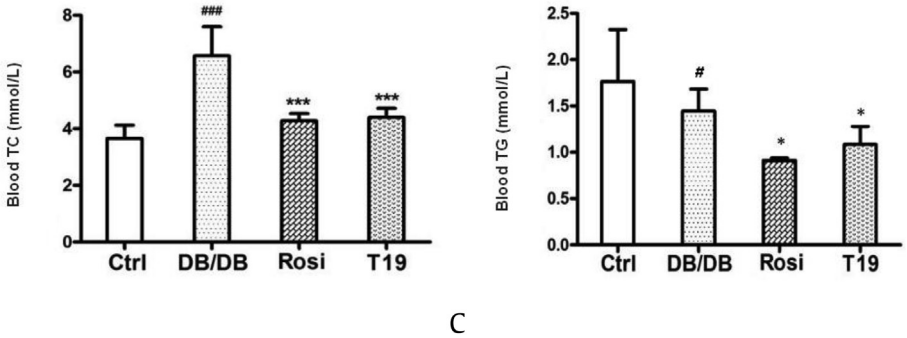

C

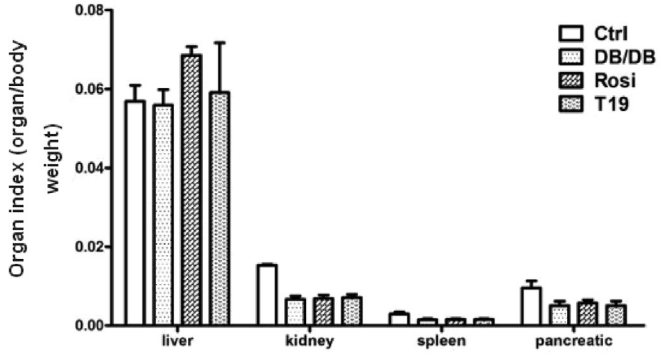

D

Fig. 5. Effects of 25-OH-PPT (T19) on serum TG and TC levels (**A**) and organ index (**B**) in STZ-induced diabetic mice (n = 10/group) and DB/DB mice (n = 6/group) (**C, D**) (Values are expressed as mean ± SEM of three independent experiments. $^{*}p < 0.05$ vs ctrl, $^{**}p < 0.01$ vs. ctrl, $^{\#}p < 0.05$ vs. model, $^{\#\#}p < 0.01$ vs. model).

3.6. Effects of 25-OH-PPT on blood lipid changes and organ index in diabetic mice

As shown in Fig. 5A, for STZ-induced diabetic mice, TG and TC levels were significantly increased by STZ injection, and both doses of 25-OH-PPT reduced TG and TC in diabetic mice with significant effects. High doses of 25-OH-PPT have good hypolipidemic function and are superior to metformin. 25-OH-PPT can significantly reduce TC and TG, and alleviate the insulin resistance caused by high TC and TG. The injection of STZ did not cause a significant change in the quality of the organ. Similarly, there was no significant change in the organ quality of the diabetic mice after 25-OH-PPT administration (Fig. 5B). For DB/DB diabetic mice (Fig. 5C), the body's total cholesterol levels increased significantly. It was found that the administration of 25-OH-PPT can reduce the total cholesterol level of DB/DB mice and restore it to a state that is not significantly different from the normal group. The effect is no different with the positive drug and has a good cholesterol lowering function. The liver of the model group increased slightly, and it also decreased after T19 administration, but it was not significant, and there was no significant change in other organs (Fig. 5D).

3.7. The protective effect of 25-OH-PPT on the liver of DB/DB mice

As shown in the Fig. 6, the liver slices of the model group have obvious fat granule enlargement and the shape of the nucleus changes. Both 25-OH-PPT and rosiglitazone can improve this condition, and the effect of 25-OH-PPT is better than that of the positive drug.

3.8. Effect of 25-OH-PPT administration on liver inflammation

As shown in Fig. 7A, in view of the above-mentioned measurement of complications (diabetes and organ index) in diabetic mice, it was found that the levels of the four inflammatory factors were significantly increased in STZ-induced diabetic mice. In the STZ mouse model, both doses of 25-OH-PPT significantly reduced the transcription levels of IL-1, IL-6 and COX-2, and the effect was significantly better than metformin, but both metformin and 25-OH-PPT had no effect on TNF-α. In the DB/DB mice model (Fig. 7B), 25-OH-PPT significantly reduced the transcription levels of IL-1, IL-6 and TNF-α. In conclusion, 25-OH-PPT has a significant inhibitory effect on the transcription of hepatic inflammatory factors, and the effect is comparable to that of the positive drug.

3.9. Effect of 25-OH-PPT administration on skeletal muscle GLUT4 and AMPK transcription levels in diabetic mice

AMPK is emerging as an important protein kinase that regulates metabolism and energy demand mainly. Activated AMPK plays important roles in increasing glucose uptake in skeletal muscle cells, increasing fatty acid oxidation, improving insulin sensitivity and regulating gene transcription. Because of its roles in regulating glucose and fatty acid metabolism, AMPK is regarded as a new pharmacological target for treatment of obesity, insulin resistance and T2DM. AMPK regulates gene expression of GLUT4. GLUT4 is an important glucose transporter. Blocking sugar transport in GLUT4 can cause severe insulin resistance. Compared with the normal mouse group (Fig. 8A), skeletal muscle AMPK was significantly decreased in the STZ-induced mouse model, and was significantly higher in the 25-OH-PPT-treated group. Although there was no significant change in skeletal muscle GLUT4 in the model group, the levels of AMPK and GLUT4 were significantly lower in the model group than in the normal group. Both levels were elevated after 25-OH-PPT administration, but not significantly so. In the DB/DB mouse model (Fig. 8B), the model group was significantly lower than the normal group in AMPK and GLUT4, and increased after 25-OH-PPT administration, but did not achieve significant results.

3.10. Effect of 25-OH-PPT administration on insulin signaling pathway protein expression in diabetic mice

For the pathogenesis of insulin resistance, the current research focus is on the expression of glucose transporter and insulin receptor substrate proteins in peripheral tissues, because the changes in the level of these are directly related to the uptake and utilization of glucose by the tissue, as well as the signal transduction. The transport of GLUT4 is also dominated by the insulin signaling pathway. IRS-1, IR and AKT are key proteins in the insulin signaling pathway, which synergistically regulate blood glucose. As shown in Fig. 8C and D, the expression of p-IR was significantly decreased in both diabetic mouse groups compared with the normal group, and

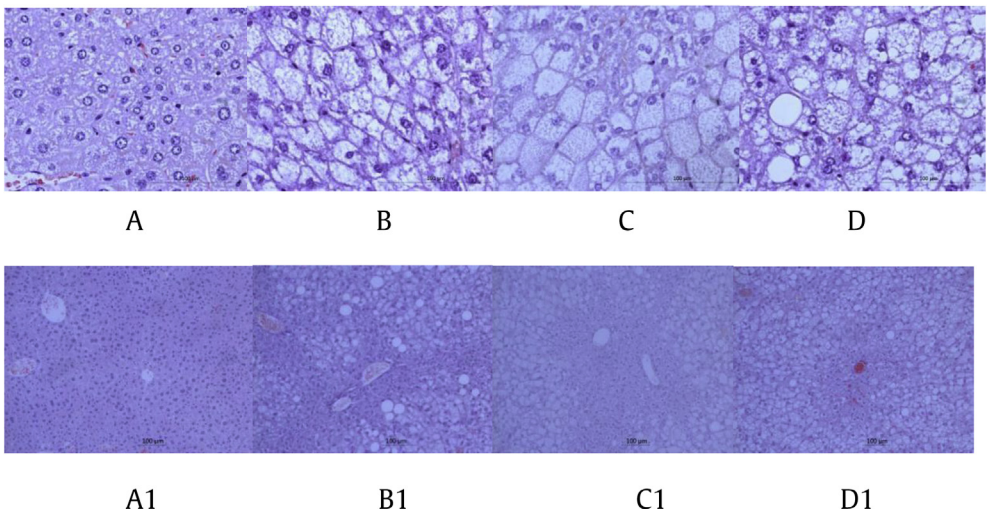

Fig. 6. Effect of 25-OH-PPT on liver pathology in DB/DB mice; **A**: blank control group 40X, **A1**: 10X; **B**: model group (DB/DB) 40X, **B1**: 10X; **C**: 25-OH-PPT group 40X, **C1**: 10X; **D**: positive drug rosiglitazone group 40X, **D1**: 10X.

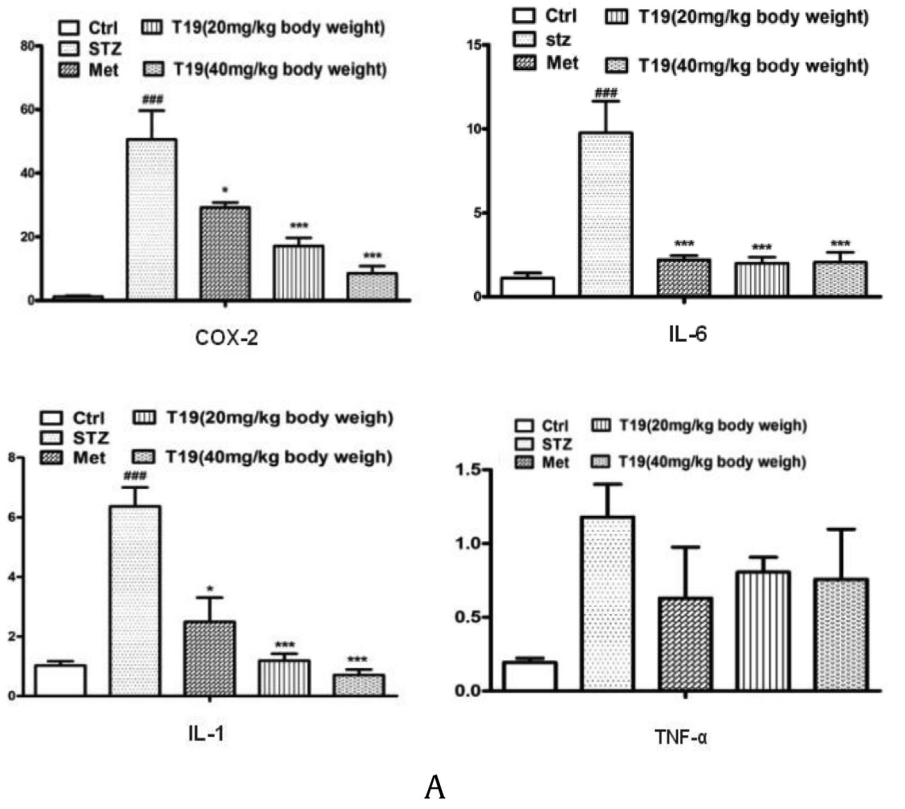

Fig. 7. Effect of 25-OH-PPT (T19) on the mRNA relative expression of hepatic inflammatory factors in STZ-induced diabetic mice (n = 10/group) (**A**) and DB/DB mice (n = 6/group) (**B**) (Values are expressed as mean ± SEM of three independent experiments. $^{*}p < 0.05$ vs. ctrl, $^{**}p < 0.01$ vs. ctrl, $^{\#}p < 0.05$ vs. model, $^{\#\#}p < 0.01$ vs. model).

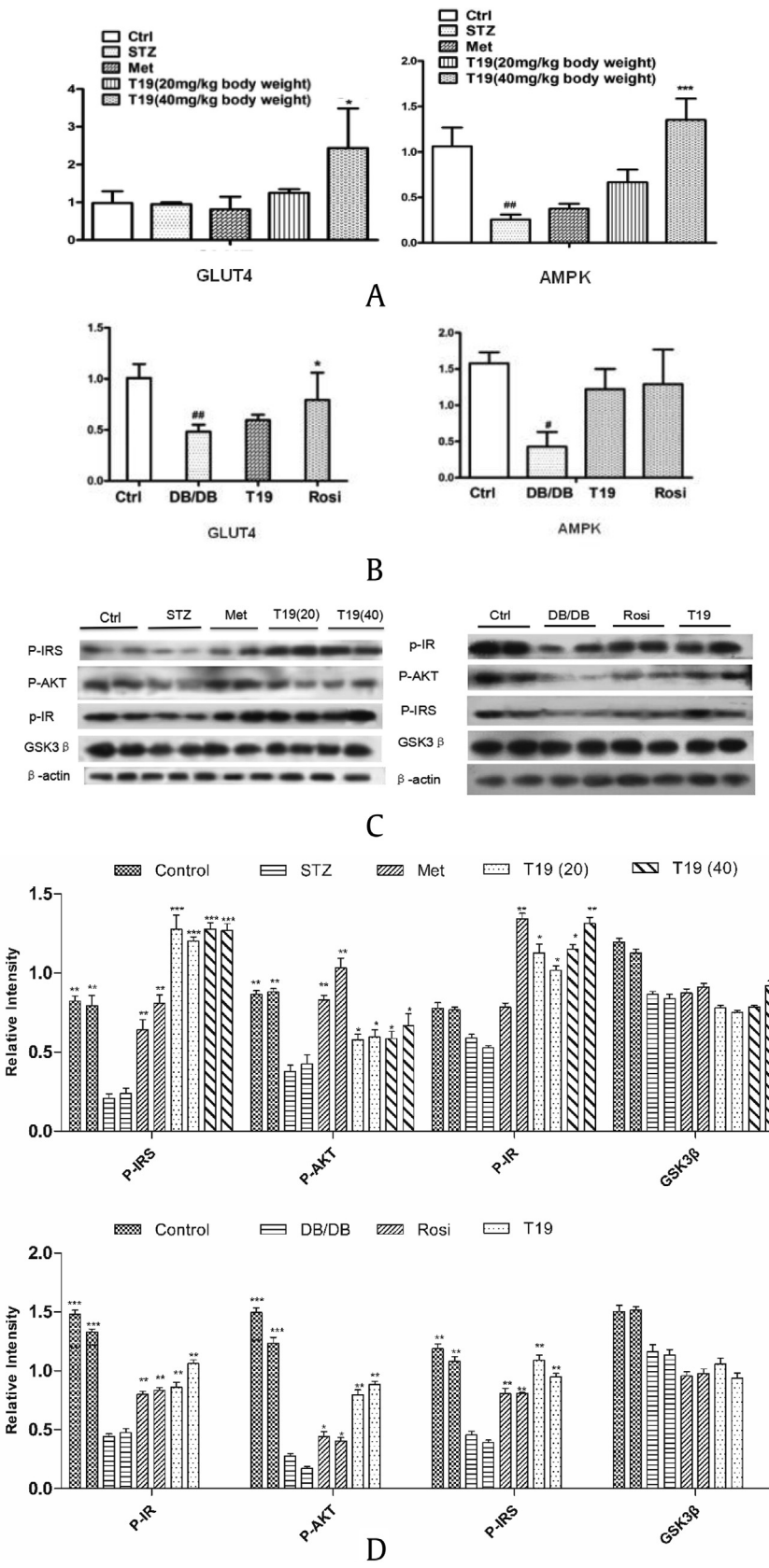

Fig. 8. Effect of 25-OH-PPT (T19) on the mRNA relative expression of GLUT4 and AMPK in skeletal muscle of STZ-induced diabetic mice (n = 10/group) (**A**) and DB/DB mice (n = 6/group) (**B**) (Values are expressed as mean ± SEM of three independent experiments. $^{*}p < 0.05$ vs. ctrl, $^{**}p < 0.01$ vs. ctrl, $^{\#}p < 0.05$ vs. model, $^{\#\#}p < 0.01$ vs. model); The effects of 25-OH-PPT (T19) on the expression of insulin signaling pathway protein in STZ-induced diabetic mice and DB/DB mice (**C**). Quantification of protein expression. (Data are presented as the means ± SEM of three independent experiments. $^{*}p < 0.05$, $^{**}p < 0.01$, $^{***}p < 0.001$ compared with model) (**D**).

the expression of downstream p-IRS and p-AKT was also decreased significantly. However, 25-OH-PPT administration was associated with increased protein expression of phosphorylated IR, IRS and p-AKT. Thus, 25-OH-PPT activated the insulin signaling pathway; improved binding of insulin, insulin-like growth factor and IR; promoted increased phosphorylation; stimulated GLUT4 transport; and enhanced glucose metabolism. There was no significant change in GSK3β in the two models, which indicated that 25-OH-PPT had no effect on total GSK3β expression and that its effect on phosphorylation should be explored further.

Using STZ modeling, STZ-induced diabetic mice had higher blood glucose concentrations. Two different doses of 25-OH-PPT were selected for testing, and metformin was used as the positive control. We found that 25-OH-PPT reduced blood glucose concentrations and body weight during the last week of administration. This may relate to the principle of STZ-induced diabetes formation. The amount of STZ applied in this experiment can damage a large number of islet cells in mice, but as the body has a certain self-repairing ability, it is speculated that the body weight is significantly reduced in the last week due to the drug and the self-repairing ability of the body. However, high 25-OH-PPT doses significantly upregulated GLUT4 and AMPK in mouse skeletal muscle in the STZ model. Both doses of 25-OH-PPT upregulated phosphorylated IR, IRS and AKT. Thus, we speculated that 25-OH-PPT can activate the insulin signaling pathway.

The hypoglycemic effect of T19 was evaluated in the DB/DB model, and rosiglitazone was selected as a positive drug. The results showed that T19 significantly reduced hyperglycemia in DB/DB mice with good stability. It also significantly enhanced glucose tolerance with an effect comparable to that rosiglitazone. However, T19 caused no obvious upregulation of GLUT4 or AMPK in skeletal muscle in the DB/DB diabetic mouse model, but can significantly increase phosphorylation of IR and IRS upstream of the insulin signaling pathway. It can be speculated that the hypoglycemic effect of T19 in the DB/DB mice model is achieved by activating the insulin signaling pathway to promote transport of GLUT4 to the cell membrane, rather than upregulating GLUT4 expression by upregulating AMPK. For both mice models, T19 has the ability to inhibit diabetic complications, which can be antiinflammatory and lipid-lowering.

4. Conclusions

In the STZ model, 25-OH-PPT increases insulin sensitivity by upregulating GLUT4 and AMPK in skeletal muscle, and activating insulin signaling pathways. In the DB/DB model, 25-OH-PPT achieves hypoglycemic effects mainly by activating the insulin signaling pathway. 25-OH-PPT has a significant effect on the treatment of diabetes complications, especially in the treatment of liver inflammation and hypolipidemic effects. This pharmacodynamic study lays the foundation for the development of a new functional food or therapeutic agent to prevent and treat diabetes.

Conflicts of interest

All the authors declare that there is no conflict of interest for any of them.

Acknowledgments

The research was supported by National Key R&D Program of China (2017YFC1702302), National Natural Science Foundation of China (81903518), Doctoral Research Startup Fund Item of Liaoning Province (2019-BS-232) and Liaoning (FGW) Engineering Technology Research Center for industrial chromatographic preparation of natural innovative drugs materials (2017-1007).

Appendix A. Supplementary data

Supplementary data to this article can be found online at https://doi.org/10.1016/j.jgr.2019.11.002.

References

[1] Venkatesh S, Reddy GD, Reddy BM, Ramesh M, Rao AVNA. Antihyperglycemic activity of Caralluma attenuta. Fitoterapia 2003;74:274–9.
[2] McKillop AM, Duffy NA, Lindsay JR, Green BD, Patterson S, O'Harte FPM, Flatt PR. Insulinotropic actions of nateglinide in type 2 diabetic patients and effects on dipeptidyl peptidase-IV activity and glucose-dependent insulinotropic polypeptide degradation. Eur J Endocrinol 2009;161:877–85.
[3] Atsuko Tanaka, Azuma Kosuke, Toyofuku Yukiko, Kurokawa Atsuko, Otsuka Aiko, Mita Tomoya, Hirosea Takahisa, Fujitani Yoshio, Miyauchi Katsumi, Daida Hiroyuki, et al. Insulin and nateglinide reduce monocyte adhesion to endothelial cells in Goto-Kakizaki rats exhibiting repetitive blood glucose fluctuation. Biochem Biophys Res Commun 2006;350:195–201.
[4] Bade A, Pizzimenti JJ. Interdisciplinary management of diabetic eye disease: a global approach to care. Internet J Allied Health Sci Pract 2007;5:1–11.
[5] Lee SH, Kang N, Kim EA, Heo SJ, Moon SH, Jeon BT, Jeon YJ. Antidiabetogenic and antioxidative effects of octaphlorethol a isolated from the brown algae Ishige foliacea in streptozotocin-induced diabetic mice. Food Sci Biotechnol 2014;23:1261–6.
[6] Li X, Wu D, Tian Y. Fibroblast growth factor 19 protects the heart from oxidative stressinduced diabetic cardiomyopathy via activation of AMPK/Nrf2/HO-1 pathway. Biochem Biophys Res Commun 2018;502:62–8.
[7] Tzatsos A, Tsichlis PN. Energy depletion inhibits phosphatidylinositol 3-kinase/Akt signaling and induces apoptosis via AMP-activated protein kinase-dependent phosphorylation of IRS-1 at Ser-794. J Biol Chem 2007;282(25):18069–82.
[8] Levine YC, Li GK, Michel T. Agonist-modulated regulation of AMP-activated protein kinase (AMPK) in endothelial cells. Evidence for an AMPK→ Rac1→ Akt→ endothelial nitric-oxide synthase pathway. J Biol Chem 2007;282(28):20351–64.
[9] Kovacic S, Soltys CL, Barr AJ, Shiojima I, Walsh K, Dyck JR. Akt activity negatively regulates phosphorylation of AMP-activated protein kinase in the heart. J Biol Chem 2003;278(41):39422–7.
[10] Attele AS, Wu JA, Yuan CS. Ginseng pharmacology: multiple constituents and multiple actions. Biochem Pharmacol 1999;58:1685–93.
[11] Jiang S, Ren DY, Li JR, Yuan GX, Li HY, Xu GY, Han X, Du PG, An LP. Effects of compound K on hyperglycemia and insulin resistance in rats with type 2 diabetes mellitus. Fitoterapia 2014;95:58–64.
[12] Zhang YZ, Su GY, Xia XY, Zhao YQ. Research progress in hypoglycemic effect of natural dammarane saponins. Chin Tradit Herb Drugs 2016;47:2758–63.
[13] Zhao YQ, Yuan CL, Fu YQ, Wei XJ, Zhu HJ, Chen YJ, Wu LJ, Li X. Chemical studies of minor triterpene compounds isolated from the stems and leaves of *Panax Ginseng C. A. Meyer*. Acta Pharm Sin 1990;25:299–301.
[14] Wang D, Chai RH, Zhao YQ. Studies on chemical constituents of the hydrolysate of the fruit of *Panax ginseng C. A. Mey*. Mod Chin. Med 2008;10:12–4.
[15] Hu HF, Han L, Zhao YQ. Studies on the chemical constituents of the hydrolysate of the stems and leaves of *Panax notoginseng (Burk.) F, H.Chen*. Mod Chin Med 2008;10:6–8.
[16] Wang K, Zhao YQ. Chemical constituents of the hydrolysate of saponins from the basal part of stem of *Panax notoginseng*. Chin J Med Chem 2008;18:288–90.
[17] Yang N, Zhang SN, Yang SL, Guo ZH, Zhang XS, Zhao YQ. The inhibition of α-glycosidase and protein tyrosine phosphatase 1B (PTP1B) activities by ginsenosides from *Panax ginseng C.A. Meyer* and simultaneous determination by HPLC-ELSD. J Funct Foods 2016;23:188–97.
[18] Hu WQ, Zhang Y, Yang N, Wang W, Cui JM, Zhao YQ. Determination of 20 (R)-25-OH-PPT in different parts of species in *Panax Linn.* by HPLC-ELSD methods. Chin Tradit Herb Drugs 2016;47:1401–4.
[19] Zhao YN, Wang ZL, Dai JG, Chen L, Huang YF. Preparation and quality assessment of high-purity ginseng total saponins by ion exchange resin combined with macroporous adsorption resin separation. Chin J Nat Med 2014;12:382–92.
[20] Liu W, Zhang S, Zu YG, Fu YJ, Ma W, Zhang DY, Kong Y, Li XJ. Preliminary enrichment and separation of genistein and apigenin from extracts of pigeon pea roots by macroporous resins. Bioresour Technol 2010;101:4667–75.

[21] Xu ZH, Ju JX, Wang K, Gu CC, Feng Y. Evaluation of hypoglycemic activity of total lignans from fructus arctii in the spontaneously diabetic goto-kakizaki rats. J Ethnopharmacology 2014;151:548–55.
[22] Yang Z, Chen CH, Zhao J, Xu WJ, He YM, Yang HJ, Zhou P. Hypoglycemic mechanism of a novel proteoglycan, extracted from Ganoderma lucidum, in hepatocytes. Eur J Pharmacol 2018;820:77–85.
[23] Jia GT, Lu XY. Enrichment and purification of madecassoside and asiaticoside from Centella asiatica extracts with macroporous resins. J Chromatogr A 2008;1193:136–41.